

A NONLINEAR CROSS-DIFFUSION EPIDEMIC WITH TIME-DEPENDENT SIRD SYSTEM: MULTISCALE DERIVATION AND COMPUTATIONAL ANALYSIS

MOHAMED ZAGOUR

ABSTRACT. A nonlinear cross-diffusion epidemic with a time-dependent Susceptible-Infected-Recovered-Died system is proposed in this paper. This system is derived from kinetic theory model by multiscale approach, which leads to an equivalent system coupled the microscopic and macroscopic equations. Subsequently, numerical investigations to design asymptotic preserving scheme property is developed and validated by various numerical tests. Finally, the numerical computational results of the proposed system are discussed in two dimensional space using the finite volume method.

1. INTRODUCTION

The outbreak of the new coronavirus, called COVID-19, caused by severe acute respiratory syndrome coronavirus 2 (SARS-CoV-2) appeared, in December 2019, apparently occurred in Wuhan, China. The spread of the epidemics has been very fast this covering all countries in the world. Thus, pandemic has severely affected the economy, health, and security of the society all over the world. Data are so impressive, as by August 2021 more than 200 million people have been infected and more than 4 million people died [1].

As it is known, mathematical models may help decision making, for example, about containment measures, lock-down, and vaccination campaigns. Indeed, they can contribute both to research in epidemiology and to crisis managers, however without naively claiming that mathematics can tackle the problem of derivation of models by a standing alone approach. For instance, models can depict a variety of epidemic scenarios. In addition, they can contribute to a deeper understanding the contagion mechanisms.

Several models have been proposed in the literature to describe the dynamic of epidemics which can be classified as network or collective models. The first class treat a population as a network of interacting individuals, and the contagion process is described at the microscopic scale see [36]. Data on the spread of the epidemics are available in [18, 24, 26]. Modeling of vaccination dynamics and medical actions are treated in [23, 33].

Collective models describe the spread of the epidemic in a population using a limited number of collective variables with a small number of parameters. For instance, celebrated logistic models [22, 34], Richards models [28], susceptible-infected-recovered (SIR) models [4, 22], and susceptible-exposed-infectious-removed (SEIR) models [15].

It is worth to mention that the classical SIR, SEIR, and other similar models belong to the class of compartmental models [12, 15, 29, 31]. An exhaustive presentation, which includes qualitative analysis and biological applications can be found in [27]. However, the the paper [16] introduces conceivable derivation of theses models as natural development of classical SEIR models. The interested reader is addressed to [6, 16] not only for a broad reference to the existing literature, but also for various challenging research perspectives.

Key words and phrases. kinetic theory; multiscale derivation; cross-diffusion; asymptotic preserving scheme; finite volume method; pattern formation.

This paper is devoted to a multiscale derivation approach of time-dependent nonlinear SIRD cross-diffusion system (2.1) from kinetic theory model by using the micro-macro decomposition method. Firstly, the kinetic theory model is rewritten as coupled system of microscopic part and macroscopic one and subsequently macroscopic models are derived by low order asymptotic expansions in terms of a small parameter. Note that this approach has been applied to the micro-macro application in different fields. For example, a time-dependent SEIRD reaction diffusion [37], chemotaxis phenomena related to Keller-Segel model [5], and formation of patterns induced by cross-diffusion in a fluid [3, 7]. This technique motivated the design numerical tools that preserve the asymptotic property [19, 21]. Concretely, these methods design the uniform stability and consistency of numerical schemes in the limit along the transition from kinetic to macroscopic regimes.

Motivated by the obtained numerical results in one dimensional space, this paper is also deals with the computational analysis in two dimensional space using finite volume method. We provide the pattern formation induced by cross-diffusion term. In the modeling point of view, the term cross-diffusion has the interpretation that the susceptible SP moves away from the increasing gradients of the infected SP. In addition, it is assumed that the cross-diffusion effect depends on the local population density. Thus, for nonlinear cross-scattering, recklessness exists at a small number and fatalism at a high total population number. With recklessness and fatalism, the susceptible subpopulation decreases its tendency to avoid the agents of the infected population.

The rest of this paper is organized as follows: in Section 2 we present a phenomenological derivation of a macro-scale model of virus contagion and cross-diffusion in space. Section 3 briefly presents the multiscale approach by micro-macro method which leads to the derivation of system (2.1) from a kinetic theory model. Section 4 is devoted to the development of an asymptotic preserving numerical scheme in one dimensional space by finite volume method. The aim is to guarantee the uniform stability with respect to Knudsen parameter ε , related to the mean distance between individuals, as well as consistency with the cross-diffusion limit. In addition, we provide some numerical simulations obtained with the equivalent micro-macro formulation and also with the macroscopic scheme, where we show the asymptotic preserving scheme property. In addition, we show the role of presence of the diffusion terms in system (2.1), and its sensitivity with respect to the different choices of the reproduction ratio R_0 . Finally, motivated by the obtained numerical results in one dimensional space, Section 5 provide numerical results in two dimensional space using finite volume method of formation of patterns.

2. PHENOMENOLOGICAL MODELING OF NONLINEAR CROSS-DIFFUSION POPULATION DYNAMICS

We consider a population constituted by N_0 individuals which can be subdivided into a number of sub-population, in short SP, each characterized by a different biological state. Specifically, we consider the following SP whose states are defined by their number, referred to N_0 , depending on time and space, where individuals correspond to:

- (1) $N(t, x)$ Alive;
- (2) $S(t, x)$ Susceptible;
- (3) $I(t, x)$ Infected;
- (4) $R(t, x)$ Recovered;
- (5) $D(t, x)$ Died.

Accordingly, the aforementioned normalization with respect to N_0 implies that

$$N(t, x) + S(t, x) + I(t, x) + R(t, x) + D(t, x) = 1, \quad t \geq 0, \quad x \in \Omega,$$

where Ω is a bounded domain within which the population is confined.

The multiscale derivation of our proposed macroscopic system can be obtained according to the following assumptions:

- (1) Individuals diffuse within the domain Ω by a nonlinear diffusion function $\varphi(x, h)$ depending on a spacial distribution which considers the preferred directions of propagation and the on density of SP;
- (2) The susceptible SP moves away from increasing gradients of the infected SP. This can be modeled by a cross-diffusion term;
- (3) The interaction dynamics is modeled by a source term involving the interactions of different SPs;
- (4) Modeling of interactions accounts uses the parameters reported in Table 1 which also reports the parameters underlying the assumptions of the interaction dynamics;
- (5) Susceptible SP may become infected due to contact with infectious individuals with a transmission rate function $\beta(t)$, while infectious SP recovers with a γ rate;
- (6) The time-dependent transmission rate function $\beta(t)$ incorporates the impact of mandatory government actions (i.e total or partial lockdown), respecting sanitary protocol and vaccination campaigns.

TABLE 1. Description of the parameters of the SIRD system with vital dynamics and constant population

Parameter	Description
A	Recruitment rate assumed $A = \mu N$
μ	Natural death rate for susceptible individuals
$\beta(t)$	Transmission rate function
γ	Recovery rate of infectious individuals

Assumptions (1)-(6), by straightforward calculations, yield the following nonlinear cross-diffusion SIRD system with vital dynamics and constant population:

$$\begin{cases} \partial_t S = d_1 \nabla \cdot (\varphi_1(x, S) \nabla S) + \nabla \cdot (\chi(S, I) \nabla I) + A - \mu S - \beta(t) S \frac{I}{N}, \\ \partial_t I = d_2 \nabla \cdot (\varphi_2(x, I) \nabla I) + \beta(t) S \frac{I}{N} - (\mu + \gamma) I, \\ \partial_t R = d_3 \nabla \cdot (\varphi_3(x, R) \nabla R) + \gamma I - \mu R, \\ \partial_t D = \alpha I, \end{cases} \quad (2.1)$$

where d_i , $i = 1, 2, 3$ are the self-diffusion coefficients considered positive constants.

Mathematical model 2.1 is implemented with the following initial and boundary conditions:

$$\begin{cases} \frac{\partial S}{\partial \nu} = \frac{\partial I}{\partial \nu} = \frac{\partial R}{\partial \nu} = 0, & x \in \partial\Omega, t > 0, \\ S(0, x) = S_0(x), I(0, x) = I_0(x), & x \in \Omega, \\ R(0, x) = R_0(x), D(0, x) = D_0(x), & x \in \Omega. \end{cases} \quad (2.2)$$

Note that if $\chi = 0$ and $\varphi_i = 1$, system (2.1) reduces to the reaction-diffusion SIR system [2, 14, 25, 35]. For instance, the authors in [2] provide a qualitative analysis to explore the impact of spatial heterogeneity of environment and human movement on the persistence and extinction of a disease. While, the authors in [14] investigate analytically and numerically the behavior of positive solutions to a spatial SIR reaction–diffusion model.

Considering a time dependent transmission function can help to well model the different strategies taken to defeat the virus, for instance partial or total lockdown and the vaccination campaign.

We mention that the basic reproduction ratio, denoted by R_0 , is the classical epidemiological measure associated with the reproductive power of the disease. It is used to estimate the growth of the viral epidemic. For our system (2.1) it is given by the following function

$$R_0(t) = \frac{\beta(t)}{\gamma + \mu}, \quad (2.3)$$

which provides a threshold for disease-free equilibrium point stability. Indeed, if $R_0(t) < 1$, the disease goes out; while if $R_0(t) > 1$, an epidemic occurs, see e.g. [20].

Recently, the author in [37] proposed a time-dependent SEIRD reaction-diffusion model with the following features : *i*) a transmission rate function rather than a constant and *ii*) the diffusion of individuals depends on a spatial distribution which considers the preferred directions of propagation modeled by a coefficient which models the diffusion coefficient in the territory. Specifically, the model takes into account both transport and diffusion and, subsequently, the modeling of these terms takes into account the specific geography of the territory and, in particular, the transport network. However, this subject has been developed in [8, 9, 11]. In this paper, basing on the afore-said paper, we proposed an improved model which takes into account the nonlinear self-diffusion depending on the density of the SP, namely $\varphi_i(x, h)$. In addition, we add the cross-diffusion term $\nabla(\chi(S, I)\nabla I)$ in the dynamic of the susceptible SP. Indeed, this allows the susceptible SP to avoid the infected SP by the added cross-diffusion term. Concretely, the cross-diffusion term directs the flow in the opposite direction of the gradient ∇I whenever there is an increase of the amount of the infected SP, consequently the susceptible SP moves away from the direction of the increasing gradient [10, 32].

3. FROM KINETIC THEORY MODEL TO SIRD CROSS-DIFFUSION SYSTEM

This sections deals with a multiscale approach to derivation of the time-dependent SIRD cross-diffusion system (2.1) from kinetic theory model on the basis of the micro-macro decomposition technique. We start with presenting the properties of the kinetic theory model. Then, we rewrite it as coupled system of microscopic part and macroscopic one. Finally, we derive macroscopic models by low order asymptotic expansions in terms of a small parameter ε that measures the distance between individuals.

3.1. Kinetic theory model. The kinetic theory model can be stated adopting the parabolic-parabolic scaling limit as follows for $i = 1, 2, 3$

$$\begin{cases} \varepsilon \partial_t f_i + v \cdot \nabla_x f_i = \frac{1}{\varepsilon} \mathcal{T}_i[f_1, \dots, f_{i-1}, f_{i+1}, \dots, f_3](f_i) + \varepsilon G_i(f_1, \dots, f_3), \\ \partial_t D = \alpha \int_V f_2 dv, \\ f_i(0, x, v) = f_{i,0}(x, v), \quad D(0, x) = D_0(x), \end{cases} \quad (3.1)$$

where $f_1(t, x, v)$, $f_2(t, x, v)$, $f_3(t, x, v)$ are the distribution functions describing the statistical evolution of susceptible, infected and recovered individuals, respectively. $t > 0$, $x \in \mathbb{R}^d$, $v \in V$ are respectively, time, position and velocity. The term \mathcal{T}_i is the stochastic operator representing a random modification of direction of individuals and the operator G_i ($i = 1, 2, 3$) describes their gain-loss balance..

The micro-macro decomposition technique is based on the following assumptions.

Assumption 1: The turning operator \mathcal{T}_i is decomposed as follows:

$$\mathcal{T}_i[f_1, \dots, f_{i-1}, f_{i+1}, \dots, f_3](f_i) = \mathcal{L}_i(f_i) + \varepsilon \mathcal{T}_i^2[f_1, \dots, f_{i-1}, f_{i+1}, \dots, f_3](f_i), \quad (3.2)$$

where \mathcal{L}_i represents the dominant part of the turning kernel and is assumed to be independent of $f_1, \dots, f_{i-1}, f_{i+1}, \dots, f_3$. The operators \mathcal{T}_i^j for $i = 1, 2, 3$ and $j = 1, 2$ are given by

$$\mathcal{T}_i^j(f_i) = \int_V (T_i^j(v^*, v) f_i(t, x, v^*) - T_i^j(v, v^*) f_i(t, x, v)) dv^*, \quad (3.3)$$

where T_i^j is the probability kernel for the new velocity $v \in V$ given that the previous velocity was v^* .

Assumption 2: We assume that the operators \mathcal{T}_i satisfy

$$\int_V \mathcal{T}_i dv = \int_V \mathcal{L}_i dv = \int_V \mathcal{T}_i^2 dv = 0, \quad i = 1, 2, 3, \quad (3.4)$$

and that there exists a bounded velocity distribution $M_i(v) > 0$ independent of t and x such that

$$T_i^1(v, v^*)M_i(v^*) = T_i^1(v^*, v)M_i(v), \quad (3.5)$$

holds.

Assumption 3: The flow produced by these equilibrium distributions vanish and M_i are normalized, i.e.

$$\int_V v M_i(v) dv = 0, \quad \int_V M_i(v) dv = 1, \quad i = 1, 2, 3. \quad (3.6)$$

Regarding the probability kernels, we assume that $T_i^1(v, v^*)$ is bounded, and there exist a constant $\sigma_i > 0$ ($i = 1, 2, 3$), such that

$$T_i^1(v, v^*) \geq \sigma_i M_i(v), \quad (3.7)$$

for all $(v, v^*) \in V \times V$, $x \in \Omega$ and $t > 0$.

Using the same arguments as in [3], the operator \mathcal{T}_i has the following properties.

Lemma 3.1. *If Assumptions 1-2-3 are satisfied. Then, the following properties of the operator \mathcal{T}_i for $i = 1, 2, 3$ holds true*

- i) The operator \mathcal{L}_i is self-adjoint in the space $L^2\left(V, \frac{dv}{M_i(v)}\right)$.
- ii) For $f \in L^2$, the equation $\mathcal{L}_i(g) = f$ has a unique solution $g \in L^2\left(V, \frac{dv}{M_i(v)}\right)$, satisfying

$$\int_V g(v) dv = 0 \iff \int_V f(v) dv = 0.$$

- iii) The equation $\mathcal{L}_i(g) = v M_i(v)$, has a unique solution denoted by $\theta_i(v)$ for $i = 1, 2, 3$.
- iv) The kernel of \mathcal{L}_i is $N(\mathcal{L}_i) = \text{vect}(M_i(v))$ for $i = 1, \dots, 3$.

3.2. The equivalent micro-macro formulation. Here we rewrite the kinetic theory model (3.1) as a coupled system of microscopic part and macroscopic one. We decompose the distribution function f_i for $i = 1, 2, 3$ as follows

$$f_i(t, x, v) = M_i(v)u_i(t, x) + \varepsilon g_i(t, x, v),$$

where

$$u_i(t, x) = \langle f_i(t, x, v) \rangle := \int_V f_i(t, x, v) dv.$$

Thus, $\langle g_i \rangle = 0$ for $i = 1, 2, 3$. Inserting f_i in the kinetic theory model (3.1) and using the above stated assumptions and properties of the turning operators, one has

$$\left\{ \begin{array}{l} \partial_t(M_i(v)u_i) + \varepsilon \partial_t g_i + \frac{1}{\varepsilon} v M_i(v) \cdot \nabla u_i + v \cdot \nabla g_i = \frac{1}{\varepsilon} \mathcal{L}_i(g_i) \\ \quad + \frac{1}{\varepsilon} \mathcal{T}_i^2[f_1, \dots, f_{i-1}, f_{i+1}, \dots, f_3](M_i u_i) + \mathcal{T}_i^2[f_1, \dots, f_{i-1}, f_{i+1}, \dots, f_3](g_i) \\ \quad + G_i(f_1, f_2, f_3) \\ \partial_t D = \alpha u_2. \end{array} \right. \quad (3.8)$$

In order to separate the macroscopic density $u_i(t, x)$ and microscopic quantity $g_i(t, x, v)$ for $i = 1, 2, 3$, we use the projection technique. For that, we consider P_{M_i} the orthogonal projection onto $N(\mathcal{T}_i)$, for $i = 1, 2, 3$. It follows

$$P_{M_i(v)}(h) = \langle h \rangle M_i(v), \quad \text{for any } h \in L^2 \left(V, \frac{dv}{M_i(v)} \right), \quad i = 1, 2, 3.$$

Consequently, inserting the operators $I - P_{M_i}$ into Eq. (3.8), using known properties for the projection P_{M_i} $i = 1, 2, 3$ and integrating this equation with respect to the variable v yields the equivalent micro-macro formulation

$$\left\{ \begin{array}{l} \partial_t g_i + \frac{1}{\varepsilon^2} v M_i(v) \cdot \nabla u_i + \frac{1}{\varepsilon} (I - P_{M_i})(v \cdot \nabla g_i) = \frac{1}{\varepsilon^2} \mathcal{L}_i(g_i) \\ \quad + \frac{1}{\varepsilon} \mathcal{T}_i^2[f_1, \dots, f_{i-1}, f_{i+1}, \dots, f_3](M_i u_i) + \mathcal{T}_i^2[f_1, \dots, f_{i-1}, f_{i+1}, \dots, f_3](g_i) \\ \quad + \frac{1}{\varepsilon} (I - P_{M_i})G_i(f_1, \dots, f_3), \\ \partial_t u_i + \langle v \cdot \nabla g_i \rangle = \langle G_i(f_1, f_2, f_3) \rangle \\ \partial_t D = \alpha u_2. \end{array} \right. \quad (3.9)$$

The micro-macro formulation (3.9) is equivalent to kinetic model (3.1) thanks to the following proposition

Proposition 3.1. *i) Let (f_1, f_2, f_3) be a solution of kinetic theory model (3.1). Then $(u_1, u_2, u_3, g_1, g_2, g_3)$ is a solution of micro-macro formulation (3.9) associated with the following initial data for $i = 1, 2, 3$*

$$u_i(t=0) = u_{i,0} = \langle f_{i,0} \rangle, \quad g_i(t=0) = g_{i,0} = \frac{1}{\varepsilon} (f_{i,0} - M_i u_{i,0}). \quad (3.10)$$

ii) Conversely, if $(u_1, u_2, u_3, g_1, g_2, g_3)$ is a solution of micro-macro formulation (3.9) associated with the following initial data $(u_{1,0}, \dots, u_{3,0}, g_{1,0}, \dots, g_{3,0})$ such that $\langle g_{i,0} \rangle = 0$. Then (f_1, f_2, f_3) is a solution of the kinetic model (3.1) with initial data $f_{i,0} = M_i u_{i,0} + \varepsilon g_{i,0}$ and we have $u_i = \langle f_i \rangle$ and $\langle g_i \rangle = 0$, for $i = 1, 2, 3$.

Now, to develop asymptotic analysis of the equivalent micro-macro formulation (3.9), the interacting operators \mathcal{T}_i^2 and G_i are assumed to satisfy the following asymptotic behavior in the limit

$$\begin{aligned} \mathcal{T}_i^2[M_1 u_1 + \varepsilon g_1, \dots, M_{i-1} u_{i-1} + \varepsilon g_{i-1}, M_{i+1} u_{i+1} + \varepsilon g_{i+1}, \dots, M_3 u_3 + \varepsilon g_3] \\ = \mathcal{T}_i^2[M_1 u_1, \dots, M_{i-1} u_{i-1}, M_{i+1} u_{i+1}, \dots, M_3 u_3] + O(\varepsilon), \end{aligned} \quad (3.11)$$

and

$$G_i(M_1(v)u_1 + \varepsilon g_1, \dots, M_3(v)u_3 + \varepsilon g_3) = G_i(M_1(v)u_1, \dots, M_3(v)u_3) + O(\varepsilon), \quad (3.12)$$

for $i = 1, 2, 3$. One can obtain a general macroscopic model as ε goes to 0 from the equivalent micro-macro formulation (3.9). Indeed, using (3.12) and (3.9), one has for $i = 1, \dots, 3$

$$\mathcal{L}_i(g_i) = v M_i(v) \cdot \nabla u_i - \mathcal{T}_i^2[M_1 u_1, \dots, M_{i-1} u_{i-1}, M_{i+1} u_{i+1}, \dots, M_3 u_3](M_i u_i)$$

From Lemma 3.1, property *ii*), the operator \mathcal{T}_i is invertible. This implies

$$g_i = \mathcal{L}_i^{-1} \left(v M_i(v) \cdot \nabla u_i - \mathcal{T}_i^2[M_1 u_1, \dots, M_{i-1} u_{i-1}, M_{i+1} u_{i+1}, \dots, M_3 u_3](M_i u_i) \right) + O(\varepsilon). \quad (3.13)$$

Inserting (3.13) into the second equation in (3.9) yields the following macroscopic system

$$\begin{aligned} \partial_t u_i + \left\langle v \cdot \nabla \mathcal{L}_i^{-1} \left(v M_i(v) \cdot \nabla u_i - \mathcal{T}_i^2 [M_1 u_1, \dots, M_{i-1} u_{i-1}, M_{i+1} u_{i+1}, \dots, M_3 u_3] (M_i u_i) \right) \right\rangle \\ = \left\langle G_i(M_1(v) u_1, M_2(v) u_2, M_3(v) u_3) \right\rangle + O(\varepsilon). \end{aligned} \quad (3.14)$$

Thanks to the following equalities

$$\left\langle v \cdot \nabla \mathcal{L}_i^{-1} \left(v M_i(v) \cdot \nabla u_i \right) \right\rangle = \nabla \cdot \left(\langle v \otimes \theta_i(v) \rangle \cdot \nabla u_i \right),$$

and

$$\begin{aligned} \left\langle v \cdot \nabla \mathcal{L}_i^{-1} \left(\mathcal{T}_i^2 [M_1 u_1, \dots, M_{i-1} u_{i-1}, M_{i+1} u_{i+1}, \dots, M_3 u_3] (M_i u_i) \right) \right\rangle \\ = \nabla \cdot \left\langle \frac{\theta_i(v)}{M_i(v)} u_i \mathcal{T}_i^2 [M_1 u_1, \dots, M_{i-1} u_{i-1}, M_{i+1} u_{i+1}, \dots, M_3 u_3] (M_i) \right\rangle \end{aligned}$$

where $\theta_i(v)$ are given in Lemma 3.1 for $i = 1, 2, 3$, one has the following general macroscopic system

$$\begin{cases} \partial_t u_i + \nabla \cdot \left(\Gamma_i(u_1, \dots, u_{i-1}, u_{i+1}, \dots, u_3) u_i - D_i \cdot \nabla u_i \right) = H_i(u_1, \dots, u_3) + O(\varepsilon), \\ \partial_t D = \alpha u_3, \end{cases} \quad (3.15)$$

where D_i and the functions Γ_i, H_i are given by

$$D_i = -\langle v \otimes \theta_i(v) \rangle, \quad (3.16)$$

$$\Gamma_i = -\left\langle \frac{\theta_i(v)}{M_i(v)} u_i \mathcal{T}_i^2 [M_1 u_1, \dots, M_{i-1} u_{i-1}, M_{i+1} u_{i+1}, \dots, M_3 u_3] (M_i) \right\rangle, \quad (3.17)$$

$$H_i(u_1, \dots, u_3) = \left\langle G_i(M_1(v) u_1, \dots, M_3(v) u_3) \right\rangle, \text{ for } i = 1, 2, 3. \quad (3.18)$$

To derive system (2.1) we consider specific choices in (3.1) of the terms that appeared in the kinetic model (3.1). Namely

$$u_1 = S, \quad u_2 = I, \quad u_3 = R.$$

The probability kernel T_i is given by

$$T_i^1 = \frac{\sigma_i}{M_i(v)}, \quad \text{for } i = 1, 2, 3.$$

This implies

$$\mathcal{L}_i(g) = -\sigma_i \left(g - M_i(v) \langle g \rangle \right) = -\sigma_i g \quad \text{for } i = 1, 2, 3. \quad (3.19)$$

Using (3.6), (3.19) and Lemma 3.1, then θ_i is given by

$$\theta_i = -\frac{1}{\sigma_i} v M_i(v).$$

The other probability kernel T_i^2 is given by

$$T_1^2[f_2](v, v^*) = \frac{\sigma_1 D_1 M_1 v}{f_1} (1 + \varphi_1(x, f_1)) \cdot \nabla \left(\frac{f_1}{M_1} \right) + K_{\frac{f_1}{M_1}, \frac{f_2}{M_2}}(v, v^*) \cdot \nabla \left(\frac{f_2}{M_2} \right),$$

$$T_2^2 = \frac{\sigma_2 D_2 M_2 v}{f_2} (1 + \varphi_2(x, f_2)) \cdot \nabla \left(\frac{f_2}{M_2} \right),$$

and

$$T_3^2 = \frac{\sigma_3 D_3 M_3 v}{f_3} (1 + \varphi_3(x, f_3)) \cdot \nabla \left(\frac{f_3}{M_3} \right),$$

where the functions $K_{\frac{f_2}{M_2}, \frac{f_2}{M_2}}$ and $\varphi_i(x, f_i)$ satisfy the following asymptotic

$$K_{u_1 + \varepsilon \frac{g_1}{M_1}, u_2 + \varepsilon \frac{g_2}{M_2}} = K_{u_1, u_2} + O(\varepsilon), \quad \varepsilon \rightarrow 0,$$

$$\varphi_i(x, u_i + \varepsilon \frac{g_i}{M_i}) = \varphi_i(x, u_i) + O(\varepsilon), \quad \varepsilon \rightarrow 0.$$

From Eq. (3.3), we obtain

$$\mathcal{T}_1^2[M_2 u_2, M_3 u_3](M_1) = -\frac{\sigma_1}{r^2} d|V| \chi(u_1, u_2) \cdot \nabla u_2,$$

where

$$\chi(u_1, u_2) = \left\langle K_{u_1, u_2}(v, v^*) M_1(v) - K_{u_1, u_2}(v^*, v) M_1(v^*) \right\rangle.$$

From (3.3) and Eq. (3.17), one has

$$\Gamma_1 = \frac{D_1}{S} (1 + \varphi_1(x, S)) \cdot \nabla S + \chi(S, I) \nabla I,$$

and

$$\Gamma_2 = \frac{D_2}{I} (1 + \varphi_2(x, I)) \cdot \nabla I, \quad \Gamma_3 = \frac{D_3}{R} (1 + \varphi_3(x, R)) \cdot \nabla R.$$

Finally, the modeling of the interaction operators G_i is given by

$$\begin{cases} G_1(f_1, f_2, f_3) = \frac{1}{|V|} (A - \mu f_1 - \beta(t) f_1 f_2 / n), \\ G_2(f_1, f_2, f_3) = \frac{1}{|V|} (\beta(t) f_1 f_2 / n - (\mu + \gamma) f_2), \\ G_3(f_1, f_2, f_3) = \frac{1}{|V|} (\gamma f_2 - \mu f_3). \end{cases} \quad (3.20)$$

Then, using the definition of H_i in (3.18) to obtain from (3.20) the following equality

$$H_i(S, I, R) = F_i(S, I, R). \quad (3.21)$$

Collecting the previous results, we obtain the time-dependent nonlinear SIRD cross-diffusion system (2.1) of the order $O(\varepsilon)$

$$\begin{cases} \partial_t S = d_1 \nabla \cdot (\varphi_1(x, S) \nabla S) + \nabla (\chi(S, I) \nabla I) + A - \mu S - \beta(t) SI / N + O(\varepsilon), \\ \partial_t I = d_2 \nabla \cdot (\varphi_2(x, I) \nabla I) + \beta(t) SI / N - (\mu + \gamma) I + O(\varepsilon), \\ \partial_t R = d_3 \nabla \cdot (\varphi_3(x, R) \nabla R) + \gamma I - \mu R + O(\varepsilon), \\ \partial_t D = \alpha I. \end{cases} \quad (3.22)$$

4. NUMERICAL ANALYSIS OF THE EQUIVALENT MICRO-MACRO FORMULATION IN ONE DIMENSIONAL SPACE

In this section, we develop an asymptotic preserving (AP)-scheme in one dimension of the equivalent micro-macro formulation developed in Section 3. This method designs uniform stability with respect to the parameter ε , related to the mean distance between individuals, as well as consistency with the nonlinear cross-diffusion limit. The discretization of micro-macro formulation (3.9) is carried out with respect to each independent variable, namely time, space and velocity.

4.1. Semi-implicit time discretization. Here we present a time discretization of micro-macro formulation (3.9). Let denote by Δt a fixed time step, and by t_k a discrete time such that $t_k = k \Delta t$ $k \in N$. The approximation of $u_i(t, x)$ and $g_i(t, x, v)$ at the time step t_k are denoted respectively by $u_i^k \approx u_i(t_k, x)$ and $g_i^k \approx g_i(t_k, x, v)$.

In the first microscopic equations of (3.9), the term $\frac{1}{\varepsilon} \mathcal{L}_i(g_i)$ presents a stiffness in the collision

part for small ε . Thus, it is natural to take an implicit scheme to ensure the stability for this term, while the other terms are still explicit. Consequently,

$$\begin{aligned}
& \frac{g_i^{k+1} - g_i^k}{\Delta t} + \frac{1}{\varepsilon^2} v M_i \cdot \nabla u_i^k + \frac{1}{\varepsilon} (I - P_{M_i})(v \cdot \nabla g_i^k) = \frac{1}{\varepsilon^2} \mathcal{L}_i(g_i^{k+1}) \\
& + \frac{1}{\varepsilon^2} \mathcal{T}_i^2[M_1 u_1^k, \dots, M_{i-1} u_{i-1}^k, M_{i+1} u_{i+1}^k, \dots, M_3 u_3^k](M_i u_i^k) \\
& + \frac{1}{\varepsilon} \mathcal{T}_i^2[M_1 u_1^k, \dots, M_{i-1} u_{i-1}^k, M_{i+1} u_{i+1}^k, \dots, M_3 u_3^k](g_i^k) \\
& + \frac{1}{\varepsilon} (I - P_{M_i}) G_i(u_1^k, u_2^k, u_3^k).
\end{aligned} \tag{4.1}$$

In the second macroscopic equations of (3.9), we take the function g at the time t_{k+1} , which gives

$$\frac{u_i^{k+1} - u_i^k}{\Delta t} + \langle v \cdot \nabla g_i^{k+1} \rangle = \langle G_i(u_1^k, u_2^k, u_3^k) \rangle. \tag{4.2}$$

Proposition 4.1. *The time discretization (4.1)-(4.2) is consistent with (3.14) in the limit.*

4.2. Fully discrete asymptotic preserving (AP)-scheme in 1D. Here we construct a suitable space discretization of (4.1)-(4.2) using finite volume method. The domain space under consideration is $[-L, L]$. Note that the velocity space in the interval $[-V, V]$ can be treated by using a standard discretization.

For this, let denote by $K_j =]x_{j-\frac{1}{2}}, x_{j+\frac{1}{2}}[$ the control volume where $x_j = \frac{1}{2}(x_{j-\frac{1}{2}} + x_{j+\frac{1}{2}})$ and its length is denoted by $h_j = x_{j+\frac{1}{2}} - x_{j-\frac{1}{2}}$ for $j = 1, \dots, N_x$, (N_x is the total number of cells). The approach consists to compute the macroscopic densities in K_j and the microscopic quantities are computed on ∂K_j as follow

$$u_i(t_k, x)|_{K_j} \approx u_{i,j}^k, \text{ and } g_i(t_k, x_{j+\frac{1}{2}}, v)|_{\partial K_j} \approx g_{i,j+\frac{1}{2}}^k, \quad i = 1, \dots, 3, \quad j = 1, \dots, N_x.$$

Then, the full discretization of the equivalent micro-macro formulation (3.9) is given as follow

$$\begin{aligned}
& \frac{g_{i,j+\frac{1}{2}}^{k+1} - g_{i,j+\frac{1}{2}}^k}{\Delta t} + \frac{1}{\varepsilon^2} v M \frac{u_{i,j+1}^k - u_{i,j}^k}{h_j} + \frac{1}{\varepsilon} (I - P_{M_i}) \left(v + \frac{g_{i,j+\frac{1}{2}}^k - g_{i,j-\frac{1}{2}}^k}{h_j} + v - \frac{g_{i,j+\frac{3}{2}}^k - g_{i,j+\frac{1}{2}}^k}{h_j} \right) \\
& = \frac{1}{\varepsilon^2} \mathcal{L}_i(g_{i,j+\frac{1}{2}}^{k+1}) + \frac{1}{\varepsilon^2} \mathcal{T}_i^2[M_1 u_{1,j+\frac{1}{2}}^k, \dots, M_{i-1} u_{i-1,j+\frac{1}{2}}^k, M_{i+1} u_{i+1,j+\frac{1}{2}}^k, \dots, M_3 u_{3,j+\frac{1}{2}}^k](M_i u_{i,j+\frac{1}{2}}^k) \\
& + \frac{1}{\varepsilon} \mathcal{T}_i^2[M_1 u_{1,j+\frac{1}{2}}^k, \dots, M_{i-1} u_{i-1,j+\frac{1}{2}}^k, M_{i+1} u_{i+1,j+\frac{1}{2}}^k, \dots, M_3 u_{3,j+\frac{1}{2}}^k](g_{i,j+\frac{1}{2}}^k) \\
& + \frac{1}{\varepsilon} (I - P_{M_i}) G_i(u_{1,j+\frac{1}{2}}^k, \dots, u_{3,j+\frac{1}{2}}^k), \\
& \frac{u_{i,j}^{k+1} - u_{i,j}^k}{\Delta t} + \left\langle v \frac{g_{i,j+\frac{1}{2}}^{k+1} - g_{i,j-\frac{1}{2}}^{k+1}}{h_j} \right\rangle = \langle G_i(u_{1,j}^k, \dots, u_{3,j}^k) \rangle,
\end{aligned} \tag{4.3}$$

where $u_{i,j+\frac{1}{2}} = \frac{u_{i,j+1} + u_{i,j}}{2}$ and $u_{i,j-\frac{1}{2}} = \frac{u_{i,j} + u_{i,j-1}}{2}$.

Proposition 4.2. *The time and space approximation (4.3) of kinetic equation (3.1) in the limit ε goes to zero satisfy the following discretization*

$$\begin{aligned}
& \frac{u_i^{k+1} - u_i^k}{\Delta t} + \frac{1}{h_j} \left\langle v \cdot \left[\mathcal{L}_i^{-1} \left(v M(v) \frac{u_{i,j+1}^k - u_{i,j}^k}{h_j} + v M(v) \frac{u_{i,j}^k - u_{i,j-1}^k}{h_j} \right. \right. \right. \\
& \quad \left. \left. \left. - \mathcal{T}_i^2 [M_1 u_{1,j+\frac{1}{2}}^k, \dots, M_{i-1} u_{i-1,j+\frac{1}{2}}^k, M_{i+1} u_{i+1,j+\frac{1}{2}}^k, \dots, M_3 u_{3,j+\frac{1}{2}}^k] (M_i u_{i,j+\frac{1}{2}}^k) \right. \right. \right. \\
& \quad \left. \left. \left. - \mathcal{T}_i^2 [M_1 u_{1,j-\frac{1}{2}}^k, \dots, M_{i-1} u_{i-1,j-\frac{1}{2}}^k, M_{i+1} u_{i+1,j-\frac{1}{2}}^k, \dots, M_3 u_{3,j-\frac{1}{2}}^k] (M_i u_{i,j-\frac{1}{2}}^k) \right) \right] \right\rangle \\
& = \langle G_i(u_{1,j+\frac{1}{2}}^k, \dots, u_{3,j+\frac{1}{2}}^k) \rangle,
\end{aligned} \tag{4.4}$$

which is consistent with the first equation of (3.13).

4.3. Boundary conditions. For the numerical solution of the kinetic equation (2.1), usually the inflow boundary conditions are prescribed as follows

$$f_i(t, x_{\min}, v) = f_{i,l}(v), \quad v > 0, \quad f_i(t, x_{\max}, v) = f_{i,r}(v), \quad v < 0, \quad \text{for } i = 1, \dots, 3.$$

Thus, the inflow boundary conditions can be rewritten in the micro-macro formulation (3.9) as follow

$$u_i(t, x_0) M_i(v) + \frac{\varepsilon}{2} (g_i(t, x_{\frac{1}{2}}, v) + g_i(t, x_{-\frac{1}{2}}, v)) = f_{i,l}(v), \quad v < 0,$$

$$u_i(t, x_{N_x}) M_i(v) + \frac{\varepsilon}{2} (g_i(t, x_{N_x+\frac{1}{2}}, v) + g_i(t, x_{N_x-\frac{1}{2}}, v)) = f_{i,r}(v), \quad v > 0.$$

We consider the following artificial Neumann boundary conditions for the other velocities

$$g_i(t, x_{\frac{1}{2}}, v) = g_i(t, x_{-\frac{1}{2}}, v), \quad v < 0,$$

$$g_i(t, x_{N_x+\frac{1}{2}}, v) = g_i(t, x_{N_x-\frac{1}{2}}, v), \quad v > 0.$$

Furthermore, the ghost points can be computed as follows

$$g_{i,j-\frac{1}{2}}^{k+1} = \begin{cases} \frac{2}{\varepsilon} \left(f_{i,l}(v) - u_{i,0}^{k+1} M_i(v) \right) - g_{i,\frac{1}{2}}^{k+1}, & v > 0, \\ g_{i,\frac{1}{2}}^{k+1}, & v < 0, \end{cases} \tag{4.5}$$

$$g_{i,N_x+\frac{1}{2}}^{k+1} = \begin{cases} \frac{2}{\varepsilon} \left(f_{i,r}(v) - u_{i,N_x}^{k+1} M_i(v) \right) - g_{i,N_x-\frac{1}{2}}^{k+1}, & v < 0, \\ g_{i,N_x-\frac{1}{2}}^{k+1}, & v > 0. \end{cases} \tag{4.6}$$

Finally, we use (4.3) to obtain

$$\left\{ \begin{aligned} & \left(1 + \frac{2\Delta t}{\varepsilon \Delta x} \langle v^+ M_i(v) \rangle \right) u_{i,0}^{k+1} = u_{i,0}^k - \frac{\Delta t}{\Delta x} \left\langle (v + v^+ - v^-) g_{i,\frac{1}{2}}^{k+1} - \frac{2v_l^+}{\varepsilon} f_l(v) \right\rangle \\ & \quad + \Delta t G_i(u_{1,0}^k, \dots, u_{3,0}^k), \\ & \left(1 - \frac{2\Delta t}{\varepsilon \Delta x} \langle v^- M_i(v) \rangle \right) u_{i,N_x}^{k+1} = u_{i,N_x}^k - \frac{\Delta t}{\Delta x} \left\langle \frac{2v^-}{\varepsilon} f_r(v) - (v - v^+ + v^-) g_{i,N_x-\frac{1}{2}}^{k+1} \right\rangle \\ & \quad + \Delta t G_i(u_{1,N_x}^k, \dots, u_{3,N_x}^k). \end{aligned} \right. \tag{4.7}$$

4.4. Numerical simulations. We provide some numerical simulations obtained with the equivalent micro-macro formulation presented in Section 4 and from the macroscopic scheme. First, we show the asymptotic preservation scheme property. Second, we provide the role of the transmission function $\beta(t)$. Next, we demonstrate the effect of the diffusion terms on the evolution of the individuals. Finally, we show the role of the presence of the cross-diffusion term by different choices of the function $\chi(S, I)$.

We consider that the velocity space is the interval $V = [-1, 1]$ with the number of grids $N_v = 164$, which can provide sufficient precision for numerical simulations [13]. The step time is $t = 10^{-3}$ and the space domain is the interval $\Omega = [-2, 2]$ with the number of cells $N_x = 200$. We take the following set of parameters as an example to analyze the results by varying some of them: $\mu = 1/83$, $\gamma = 1/3$, $\chi = 0.01$. Three cases of the diffusion coefficients are considered: i) without diffusion ($d_i = 0$), ii) with diffusion, namely $d_1 = 0.05$, $d_2 = 0.025$, $d_3 = 0.001$ and $d_4 = 0$, the same as Reference [30] where the functions $\varphi_i(x) = |x|$, and iii) same as the case ii) with diffusion coefficient depending on x , namely $\varphi_i(x) = 1 + 0.5x$. Finally, we take the following initial conditions:

$$i) \quad \begin{cases} S_0 = 2.6 \left(\exp(-(\frac{x-0.5}{0.12})^2) + \exp(-(\frac{x+0.5}{0.12})^2) \right) / (0.9\pi), \\ I_0 = 0.04 \exp(-2x^2), \\ R_0 = 0, \\ N_0 = S_0 + I_0, \end{cases}$$

$$ii) \quad \begin{cases} S_0 = 0.96 \exp(-10(\frac{x}{1.4})^2), \\ I_0 = 0.04 \exp(-2x^2), \\ R_0 = 0, \\ N_0 = S_0 + I_0. \end{cases}$$

4.4.1. Test 1: Asymptotic preserving property. In this test we aim to validate the asymptotic preserving numerical scheme property. We consider the initial conditions i), the diffusion case b) and the reproduction ratio is $R_0 = 2$.

In Figure 1, we present the plots in log scale of the error estimates given by

$$e_{\Delta x}(h) = \frac{|h_{\Delta x}(t) - h_{2\Delta x}(t)|_1}{|h_{2\Delta x}(0)|_1}$$

to test the convergence of our scheme. This can be considered as an estimation of the relative error in l^1 norm, where $h_{\Delta x}$ is the numerical solution computed from a uniform grid of size $\Delta x = \frac{x_{max} - x_{min}}{N_x}$. The computations are performed with $N_x = \{80, 160, 320, 640\}$, $\Delta t = 10^{-6}$ at $t = 0.01$ for $\varepsilon = \{1, 10^{-2}, 10^{-3}, 10^{-6}\}$.

Figure 2 shows the numerical results of susceptible, infected and recovered individuals obtained with micro-macro scheme presented in Sec. 4 and with macroscopic numerical scheme at successive instants $t = 0.5, 1, 5, 10$. The obtained numerical results have almost the same profiles in the limit when the parameter $\varepsilon = 2 \times 10^{-k}$, with $k = 0, 1, 2, 3, 4, 6$, goes to zero. This confirms that the asymptotic preserving numerical scheme is uniformly stable along the transition from kinetic regime to macroscopic regime, which illustrates the result in Proposition 4.2.

4.4.2. Test 2: Time-dependent effect by $\beta(t)$. The aim is to illustrate the transmission rate function influence over the evolution of the pandemic. For this, we start by considering constant values of $\beta = 0.1727, 0.2763, 0.449, 0.6908, 0.1.7269, 5.1807$, (the corresponding reproduction ratio is $R_0 = 0.5, 0.8, 1.3; 2, 5, 10, 15$ respectively). Figure 3 shows the variation over time of susceptible, infected and recovered individuals with diffusion case b) at $x = 0$ performed with the initial condition i). It is clear that for low values of the transmission rate, the proportion of infected individuals is low. Moreover, the steady-state results in a relatively low proportion of the population among

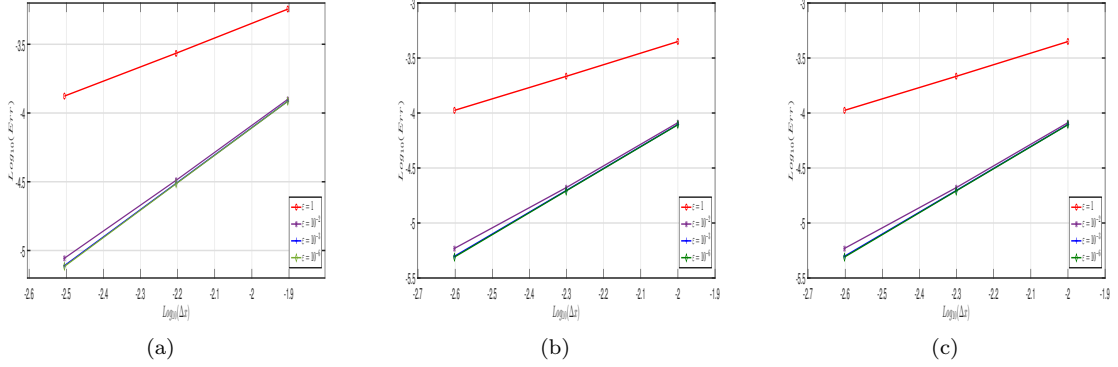


FIGURE 1. Convergence order of the method for $\varepsilon = \{1, 10^{-2}, 10^{-3}, 10^{-6}\}$ at time $t = 0.01$ ($M = 1$) for the density S in the left, the density I in the middle and the density R in the right obtained from the asymptotic preserving numerical scheme.

recovered individuals, while the majority of the population remains among susceptible individuals. While, for relatively high and moderate values of β , a large proportion of individuals is found in equilibrium among the individuals recovered. In other words, most of the population caught the disease and got infected, and then recovered. Note that, in this case, only a relatively small proportion of the population remains susceptible individuals. In addition, infected individuals disappear after a reasonable period of time, while susceptible and recovered individuals reach a non-zero constant at steady-state.

Now, let consider a time-dependent transmission rate $\beta(t)$ giving by the following step-wise function

$$\beta(t) = 0.17271\mathbb{1}_{[0, T/4]}(t) + 1.10521\mathbb{1}_{]T/4, T/2]}(t) + 0.06911\mathbb{1}_{]T/2, 2T/4]}(t) + 17.26911\mathbb{1}_{]2T/4, T]}(t), \quad (4.8)$$

where $T = 10^5$.

Figure 4 presents time variation of infected and died individuals obtained with the asymptotic preserving numerical scheme with $\varepsilon = 10^{-6}$, self-diffusion case *b*) and initial condition *ii*) at $x = 0$. We observe the numbers of infected and died individuals increase from the time $T/4$ called the first wave, also at time $t > 3T/4$ considered as the second wave occurs because of the values of β which corresponds to $R_0(t) > 1$. As time progresses, we notice that the numbers of infected and died individuals decrease at time $t > T/2$, the same at time $t < T/4$, thanks to the choice of transmission rate function, where a small value of $R_0(t) = 0.2 < 1$ and $R_0(t) = 0.1 < 1$, respectively is considered.

4.4.3. Test 3: self-diffusion effect by $\phi(x)$. This test shows the effect of self-diffusion over the interacting individuals. For this, let consider the initial conditions *ii*) and the reproduction ratio is $R_0 = 2$. In Figure 5, we show the numerical results of susceptible, infected and recovered individuals obtained with asymptotic preserving scheme where $\varepsilon = 10^{-6}$. Three cases are considered: without diffusion, case *a*) illustrated in sub-figures (a)-(b)-(c), with diffusion case *b*) illustrated in sub-figures (d)-(e)-(f)), and with diffusion case *c*) illustrated in sub-figures (h)-(g)-(i). In the first case, the individuals are all centered around the axis $x = 0$. In the second case where $\varphi_i = |x|$, we observe that individuals are more spreading within the domain. In the third case where $\varphi_i(x) = 1 + 0.5x$, we notice that the individuals diffuse more on the positive x -axis.

4.4.4. Test 4: cross-diffusion effect by $\chi(S, I)$. In this test we show the effect of the cross-diffusion term over the interacting individuals. For this, we consider the initial conditions *ii*) and the reproduction ratio is $R_0 = 2$. Figure 5 illustrates the numerical results of susceptible, infected

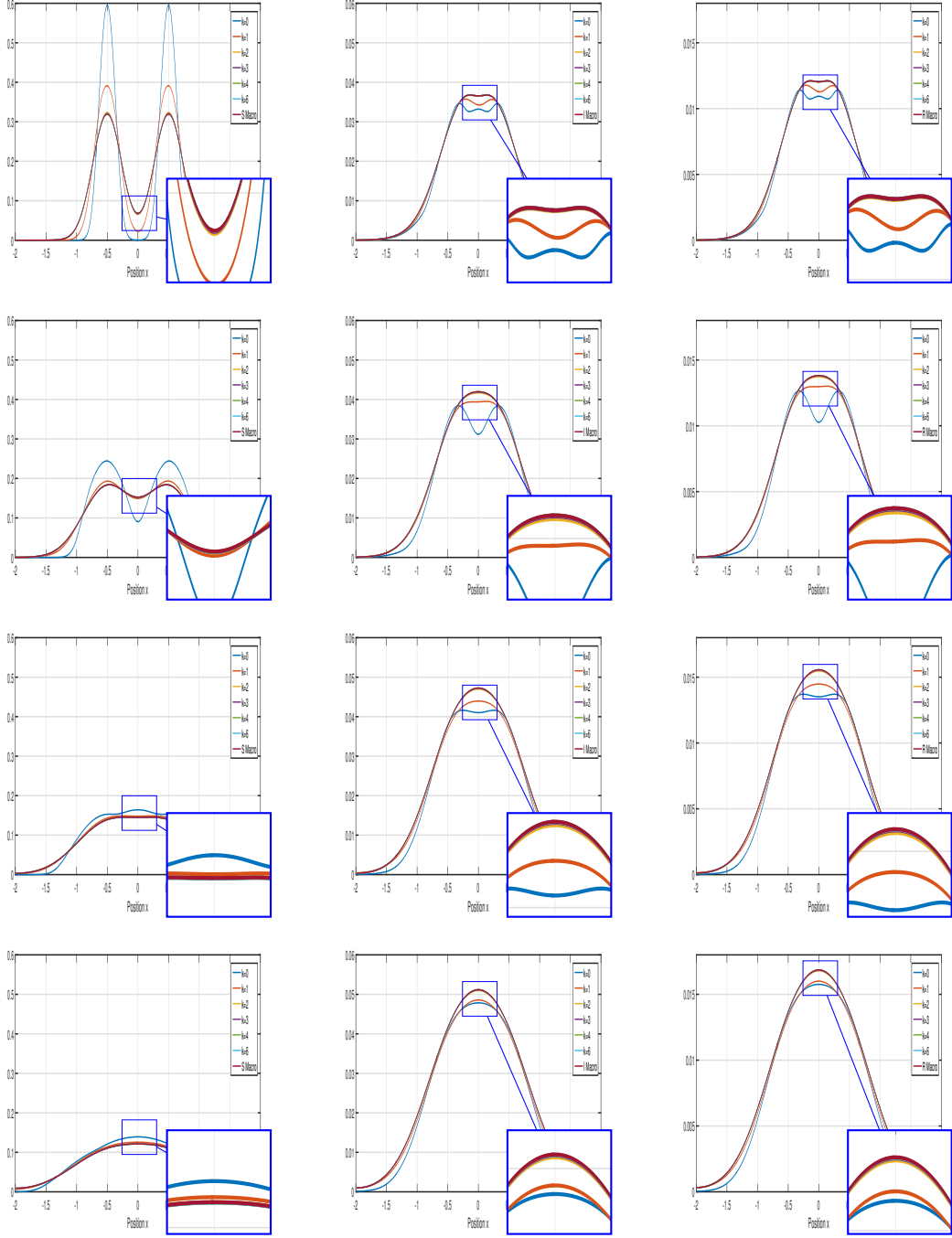


FIGURE 2. Dynamics of the densities f_1 (first column), f_2 (second column) and f_3 (third column) obtained with the asymptotic preserving numerical scheme for $\varepsilon = 2 \times 10^{-k}$, $k = 0, 1, 2, 3, 4, 6$ and with the macroscopic numerical scheme using initial conditions i) at successive time $t = 0.5, 1, 5, 10$.

and recovered individuals obtained with asymptotic preserving scheme where $\varepsilon = 10^{-6}$. Three cases are considered: without cross-diffusion where $\chi = 0$ illustrated in sub-figures (a)-(d), with cross-diffusion where $\chi = 0.01$ illustrated in sub-figures (d)-(e), and with cross-diffusion where $\chi(S) = \frac{5S}{1+S^2}$ illustrated in sub-figures (c)-(f).

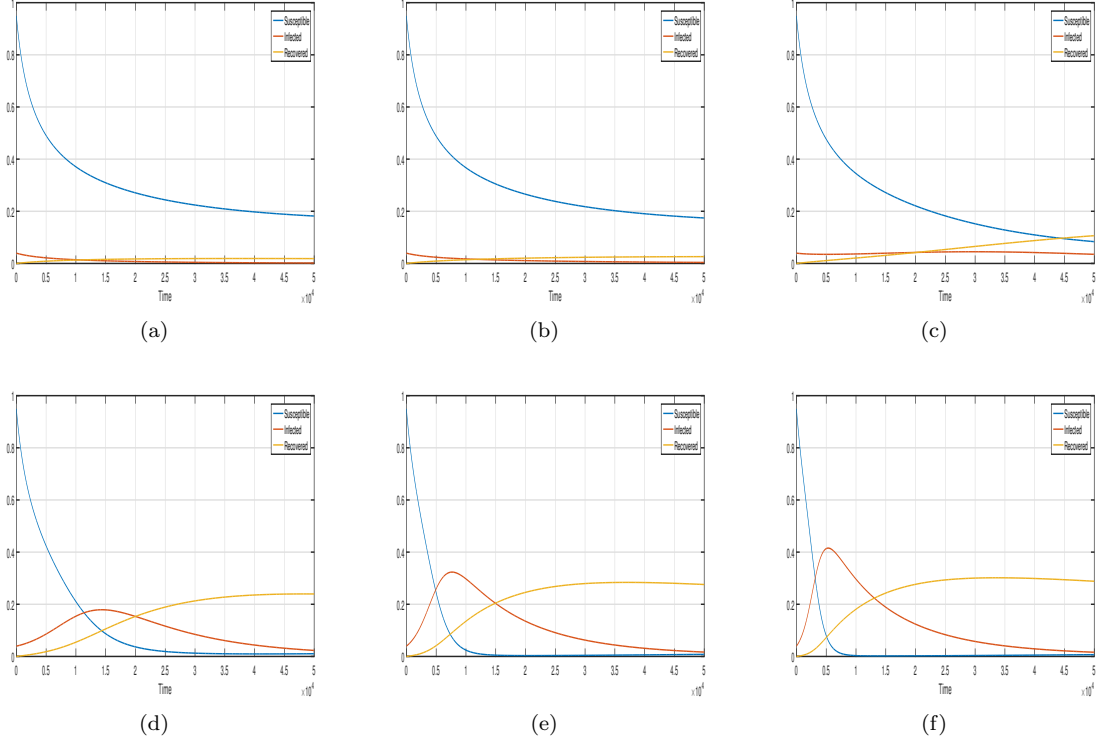


FIGURE 3. Time variation of the obtained numerical solutions from (AP)-scheme with $\varepsilon = 10^{-6}$ using initial condition *ii*) and with diffusion, at $x = 0$, for the transmission rate values $\beta = 0.1727, 0.2763, 0.449, 0.6908, 0.1.7269, 5.1807$, the corresponding reproduction ratio is $R_0 = 0.5, 0.8, 1.3; 2, 5, 10, 15$

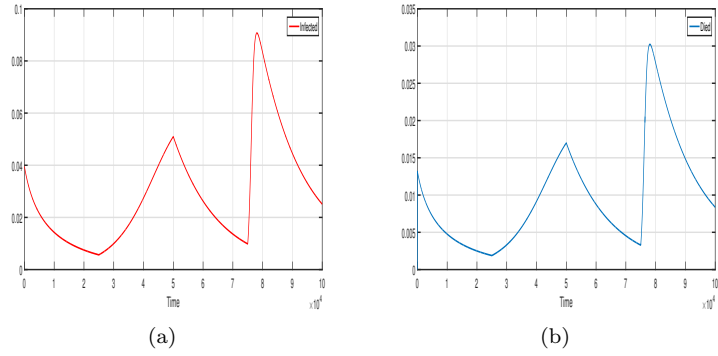


FIGURE 4. Time variation of infected a and died b individuals obtained with asymptotic preserving numerical scheme using initial condition *ii*) and diffusion case *b*), at $x = 0$. The transmission rate function $\beta(t)$ is given by Eq. (4.8) and $\varepsilon = 10^{-6}$.

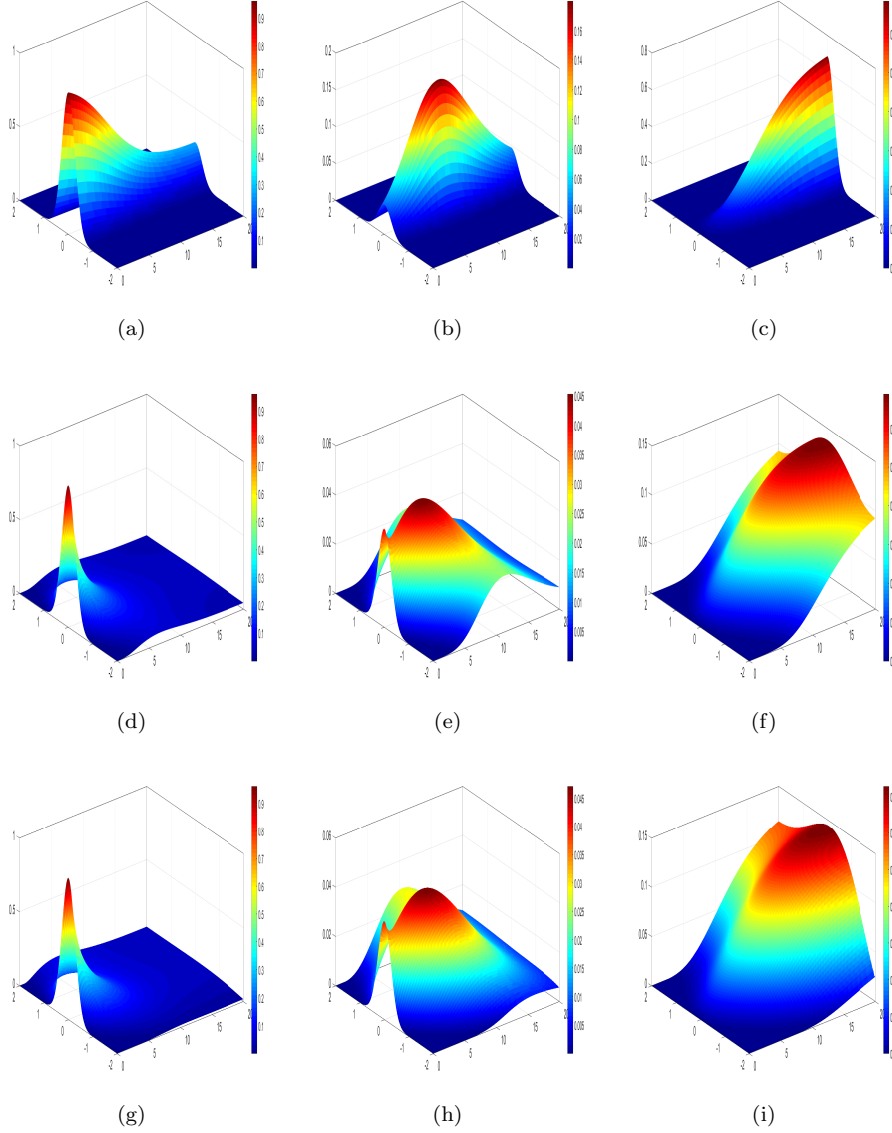


FIGURE 5. Evolution of densities f_1 (first column) f_2 (second column) and f_3 (third column) obtained with the asymptotic preserving numerical scheme for $\varepsilon = 10^{-6}$ and initial condition ii : without diffusion case a) (first line), with diffusion case b) (second line), and with diffusion case c) (third line). The reproduction ratio is $R_0 = 2$.

5. COMPUTATIONAL ANALYSIS OF SIRD CROSS-DIFFUSION EPIDEMIC SYSTEM IN TWO DIMENSIONAL SPACE

Motivated by the numerical simulations in one dimension, we illustrate the behavior of time dependent nonlinear SIRD cross-diffusion epidemic system. Namely, we show the generated formation of patterns. The numerical investigation is performed using the finite volume method.

5.1. An implicit finite-volume scheme. In order to solve numerically system (2.1), we adopt the finite volume method in 2D. For that, we consider a family \mathcal{T}_h of admissible meshes of the domain Ω consisting of disjoint open and convex polygons called control volumes, see [17]. In

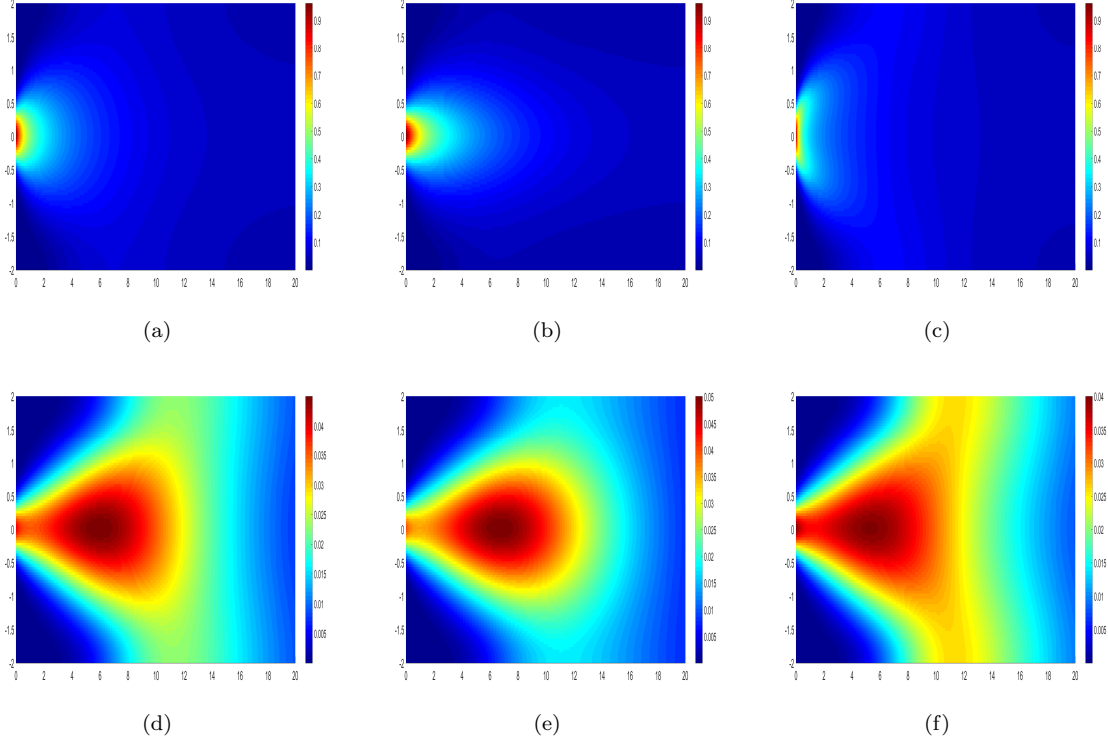


FIGURE 6. Time variation of the obtained numerical solutions of Susceptible (first line) and Infected (second line) with (AP)-scheme with $\varepsilon = 10^{-6}$ using initial condition ii) and with diffusion, at $x = 0$, for different choices of $\chi(S, I) = 0$ (left), $\chi(S, I) = 0.01$ (middle), $\chi(S, I) = \frac{5S}{1+S^2}$.

the rest of this subsection, we shall use the following notation: the parameter h is the maximum diameter of the control volumes in \mathfrak{T}_h . K is a generic volume in \mathfrak{T} , $|K|$ is the 2-dimensional Lebesgue measure of K and $N(K)$ is the set of the neighbors of K . In addition, for all $L \in N(K)$, we denote by $\sigma_{K,L}$ the interface between K and L where L is a generic neighbor of K . $\eta_{K,L}$ is the unit normal vector to $\sigma_{K,L}$ outward to K . For an interface $\sigma_{K,L}$, $|\sigma_{K,L}|$ will denote its 1-dimensional measure. $d_{K,L}$ denotes the distance between x_K and x_L , where the points x_K and x_L are respectively the center of K and L . We assume that a discrete function on the mesh \mathfrak{T}_h is a set $(w_K)_K \in \mathfrak{T}$ and we identify it with the piece-wise constant function w_h on Ω such that $w_h|_K = w_K$. Furthermore, we consider an admissible discretization of $(0, T) \times \Omega$ consisting of an admissible mesh \mathfrak{T}_h of Ω and of a time step size $\Delta t_h > 0$ (both Δt_h and the size $\max_{K \in \mathfrak{T}_h} \text{diam}(K)$ tend to zero as $h \rightarrow 0$). Now, let define the discrete gradient $\nabla_h w_h$ as the constant per diamond $T_{K,L}$ function by

$$(\nabla_h w_h)|_{\mathfrak{T}_{K,L}} = \nabla_{K,L} w_h := \frac{w_L - w_K}{d_{K,L}} \eta_{K,L}.$$

Finally, we define the average of source terms $F_{i,K}^{n+1}$ by $F_{i,K}^{n+1} = F_i(S(t^n, x), I(t^n, x), R(t^n, x))$, for $i = 1, 2, 3$. And we make the following choice to approximate the function $\chi_{K,L}^{n+1}$

$$\chi_{K,L}^{n+1} = \chi(\min\{S_K^{n+1+}, S_L^{n+1+}\}, \min\{I_K^{n+1+}, I_L^{n+1+}\}),$$

where $u_{i,J}^{n+1+} = \max(0, u_{i,J}^{n+1})$ for $i = 1, 2, 3$ and $J = K, L$. The computation starts from the initial cell averages $u_{i,0}^K = \frac{1}{|K|} \int_K u_{i,0}(x) dx$ for $i = 1, 2, 3$. To advance the numerical solution from t^n to $t^{n+1} = t^n + \Delta t$, we use the following implicit finite volume scheme: determine S_K^{n+1} , I_K^{n+1} , R_K^{n+1}

and D_K^{n+1} for $K \in \mathfrak{T}$ such that

$$\begin{cases} |K| \frac{S_K^{n+1} - S_K^n}{\Delta t} - d_1 \sum_{L \in N(K)} \frac{|\sigma_{K,L}|}{d_{K,L}} (S_L^{n+1} - S_K^{n+1}) \\ \quad + \sum_{L \in N(K)} \frac{|\sigma_{K,L}|}{d_{K,L}} \left[\chi_{K,L}^{n+1} (S_L^{n+1} - S_K^{n+1}) + \chi_{K,L}^{n+1} (I_L^{n+1} - I_K^{n+1}) \right] = |K| F_{1,K}^n, \\ |K| \frac{I_K^{n+1} - I_K^n}{\Delta t} - d_2 \sum_{L \in N(K)} \frac{|\sigma_{K,L}|}{d_{K,L}} (I_L^{n+1} - I_K^{n+1}) = |K| F_{2,K}^n, \\ |K| \frac{R_K^{n+1} - R_K^n}{\Delta t} - d_3 \sum_{L \in N(K)} \frac{|\sigma_{K,L}|}{d_{K,L}} (R_L^{n+1} - R_K^{n+1}) = |K| F_{3,K}^n, \\ |K| \frac{D_K^{n+1} - D_K^n}{\Delta t} = \alpha I_K^{n+1}, \end{cases} \quad (5.1)$$

for all $K \in \mathfrak{T}_h$, $n \in N_h$. We consider implicitly the homogeneous Neumann boundary condition and Newton method has been used in order to solve the corresponding nonlinear system arising from the implicit finite volume scheme (5.1). Note that the linear systems involved in Newton's method are solved by the GMRES method.

5.2. Numerical simulations. The numerical simulations are performed by uniform mesh given by a Cartesian grid $N_x = N_y = 200$ in the space domain $\Omega = (0, 0.5) \times (0, 0.5)$. The time stepping is explicit with a fixed time step $\Delta t = 0.001$. The model parameters are set to $\mu = 1/83$, $\gamma = 1/3$, $R_0 = 5$, the constant self coefficients are chosen to be $d_1 = 0.025$, $d_2 = 0.015$, $d_3 = 0.001$, and cross-diffusion term is given by $\chi(S) = \frac{5S}{1+S^2}$. We mention that the patterns of the species S coincide with those of I , therefore they are not shown.

5.2.1. Example 1. We assume that the density of sub populations is a random perturbation around the endemic stationary state (S^*, I^*, R^*) . Thus, the initial data are given by

$$S(0, x) = S^* + S(x)_\delta, \quad I(0, x) = I^* + I(x)_\delta, \quad R(0, x) = R^* + R(x)_\delta, \quad x \in \Omega,$$

where $J(x)_\delta \in [0, 1]$ is a uniform distributed variable for $J = S, I, R$. The stationary state is given by

$$(S^*, I^*, R^*) = ((\gamma + \mu)/\beta, \mu(R_0 - 1)/\beta, \gamma(R_0 - 1)/\beta).$$

In Figure 7, we observe islands of high concentration of susceptible individuals are formed. In fact, this reflects the phase separation triggered by the susceptible subpopulation avoiding the infected subpopulation.

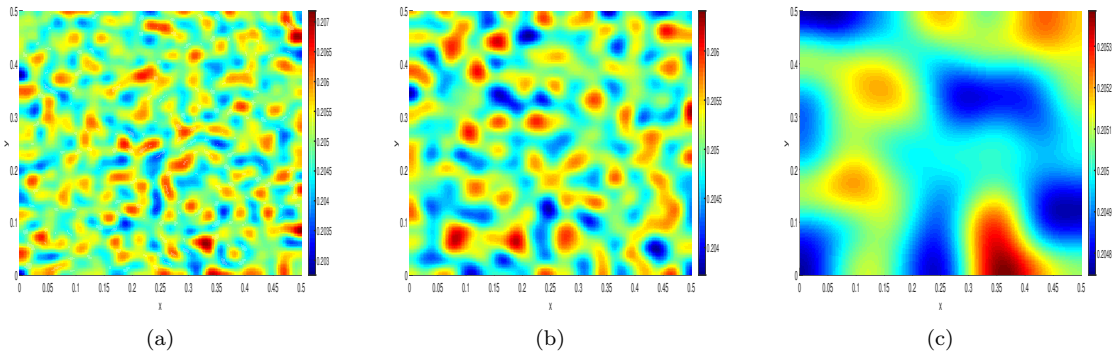


FIGURE 7. Numerical solution for S at time instants $t = 0.005, t = 0.01$ and $t = 0.1$ (Example 1).

5.2.2. *Example 2.* For this Example, the only difference from Example 1 is that the initial data is now randomly distributed at only four spatial points as follows

$$S(0, x) = S^* + \sum_{i=1}^4 S(x_i)_\delta, \quad I(0, x) = I^* + \sum_{i=1}^4 I(x_i)_\delta, \quad R(0, x) = R^* + \sum_{i=1}^4 R(x_i)_\delta, \quad x \in \Omega,$$

where $x_1 = (1/8, 1/8)$, $x_2 = (3/8, 1/8)$, $x_3 = (1/8, 3/8)$, $x_4 = (3/8, 3/8)$.

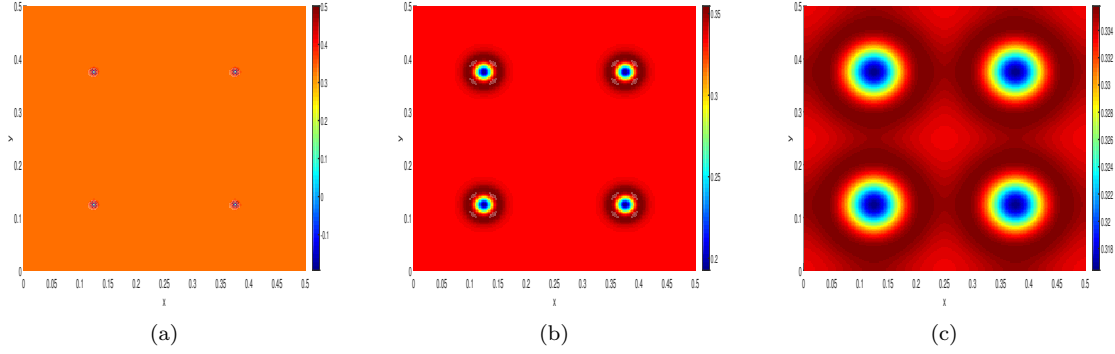


FIGURE 8. Numerical solution for S at time instants $t = 0.0001, t = 0.005$ and $t = 0.05$ (Example 2).

In Figure 8, we notice that the perturbation in four single point leads to pattern formation in the whole domain and the spatial patterns become clearly visible at earlier time steps.

6. CONCLUSION AND PERSPECTIVES

In this paper, a time-independent SIRD nonlinear cross-diffusion system for epidemic has been proposed and derived from a kinetic theory model by using multiscale approach. Several numerical simulations have been provided. Specifically, the uniform stability along the transition from kinetic to macroscopic regimes is shown and the sensitivity to the transmission rate is demonstrated where the epidemic waves are depicted. Moreover, it has shown that the presence of the self and cross-diffusion terms in system (2.1) influences the spreading of the pandemic. In addition, we provided numerical simulations in two dimensional space where the generated formation of patterns are presented in two examples.

We believe that this paper opens such interesting perspectives: For instance, extension of the proposed macroscopic model by considering a time-space diffusion $d_i(t, x)$ and the rate transmission $\beta(t, x)$.

REFERENCES

- [1] Available online: <https://www.worldometers.info/coronavirus> (accessed on August, 23 2021).
- [2] L.J.S. Allen, B.M. Bolker, Y. Lou and A.L. Nevai,, *Asymptotic profiles of the steady states for an SIS epidemic reaction-diffusion model*, Discrete Contin. Dyn. Syst., 21, (2008), pp. 1–20.
- [3] A. Atlas, M. Bendahmane, F. Karami, D. Meskine and M. Zagour, *Kinetic-fluid derivation and mathematical analysis of nonlocal cross-diffusion-fluid system*, Appl. Math. Model., 82, (2020), pp. 379–408.
- [4] N. T. J. Bailey, *The mathematical theory of infectious diseases and its applications*, New York, NY, USA: Hafner Press, 2nd ed., 1975.
- [5] N. Bellomo, A. Bellouquid, J. Nieto and J. Soler, *On the asymptotic theory from microscopic to macroscopic tissue models: an overview with perspectives*, Math. Models Methods Appl. Sci., 22, (2012), paper n. 1130001.
- [6] N. Bellomo, R. Bingham, M.A. Chaplain, G. Dosi, G. Forni, D.A. Knopoff, J. Lowengrub, R. Twarock and M.E. Virgillito, *A multi-scale model of virus pandemic: heterogeneous interactive entities in a globally connected world*, Math. Models Methods Appl. Sci., 30(8), (2020), pp. 1591–1651.
- [7] M. Bendahmane, F. Karami and M. Zagour, *Kinetic-fluid derivation and mathematical analysis of the cross-diffusion-brinkman system*, Math. Methods Appl. Sci., 41(16), (2018), pp. 6288–6311.

- [8] H. Berestycki, J.M. Roquejoffre and L. Rossi, *Propagation of epidemics along lines with fast diffusion*, Bull. Math. Biol., 83(2), (2021).
- [9] G. Bertaglia and L. Pareschi, *Hyperbolic models for the spread of epidemics on networks: kinetic description and numerical methods*, ESAIM: M2AN, 55(2), (2021), pp. 381–407.
- [10] S. Berres and Ricardo Ruiz-Baier, *A fully adaptive numerical approximation for a two-dimensional epidemic model with nonlinear cross-diffusion*, Nonlinear Anal. Real World Appl., 12(5), (2011), pp. 2888–2903.
- [11] W. Boscheri, G. Dimarco and L. Pareschi, *Modeling and simulating the spatial spread of an epidemic through multiscale kinetic transport equations*, Math. Models Methods Appl. Sci., 6(31), (2021), pp. 1059–1097.
- [12] F. Brauer, *Mathematical epidemiology: Past, present, and future*, Infect. Dis. Model., 2(2), (2017), pp. 113–127.
- [13] J.A. Carrillo and B. Yan, *An asymptotic preserving scheme for the diffusive limit of kinetic systems for chemotaxis*, Multiscale Model. Simul., 11(1), (2013), pp. 336–361.
- [14] S. Chinviriyasit and W. Chinviriyasit, *Numerical modelling of an SIR epidemic model with diffusion*, Appl. Math. Comput. 216, (2010), pp. 395–409.
- [15] G. Chowell, *Fitting dynamic models to epidemic outbreaks with quantified uncertainty: A primer for parameter uncertainty, identifiability, and forecasts*, Infect. Dis. Model., 2(3), (2017), pp. 379–398.
- [16] E. Estrada, *COVID-19 and SARS-CoV-2. Modeling the present, looking at the future*, Phys. Rep., 869, (2020), pp. 1–51.
- [17] R. Eymard, T. Gallouët and R. Herbin, *Finite Volume Methods*, in: P.G. Ciarlet, J.L. Lions (Eds.), Handbook of Numerical Analysis, vol. VII, North-Holland, Amsterdam, 2000, pp. 713–1020.
- [18] G.J. Fox, J.M. Traue and E. McBryde, *Modelling the impact of COVID-19 on intensive care services in New South Wales*, Med. J. Aust., 212, (2020), pp. 468–469.
- [19] S. Jin, *Efficient asymptotic-preserving (AP) schemes for some multiscale kinetic equations*, SIAM J. Sci. Comput., 21(2), (1999), pp. 441–454.
- [20] H. W. Hethcote, *The mathematics of infectious diseases*, SIAM Rev., 42(4), (2000), pp. 599–653.
- [21] A. Klar, *Asymptotic-induced domain decomposition methods for kinetic and drift diffusion semiconductor equations*, SIAM J. Sci. Comput., 19, (1998), pp. 2032–2050.
- [22] W. Kermack and A. McKendrick, *A contribution to the mathematical theory of epidemics*, Proc. R. Soc. Lond., A 115, (1927), pp. 700–721.
- [23] Q. Li, B. Tang, N.L. Bragazzi, Y. Xiao and J. Wu, *Modeling the impact of mass influenza vaccination and public health interventions on COVID-19 epidemics with limited detection capability*, Math. Biosci., 325, (2020), pp. 108378.
- [24] Q. Lin, S. Zhao, D. Gao, Y. Lou, S. Yang, S.S. Musa, M.H. Wang, Y. Cai, W. Wang, L. Yang and D. He, *A conceptual model for the outbreak of Coronavirus disease 2019 (COVID-19) in Wuhan, China with individual reaction and governmental action*, Int. J. Infect. Dis., 93, (2020), pp. 211–216.
- [25] Y. Lou and X.Q. Zhao, *A reaction-diffusion malaria model with incubation period in the vector population*, J. Math. Biol., 62, (2011), pp. 543–568.
- [26] L. Pang, S. Liu, X. Zhang, T. Tian and Z. Zhao, *Transmission dynamics and control strategies of covid-19 in Wuhan, China*, J. Biol. Systems, 28(3), (2020), pp. 543–560.
- [27] B. Perthame, *Transport equations in biology*, Blackwell Science Ltd, 1998.
- [28] F. J. Richards, *A flexible growth function for empirical use*, J. Exp. Bot., 10(2), (1959), pp. 290–301.
- [29] G. Röst, *SEIR epidemiological model with varying infectivity and infinite delay*, Math. Biosci. Eng., 5(2), (2008), pp. 389–402.
- [30] M. Samsuzzoha, M. Singh and D. Lucy, *Numerical study of an influenza epidemic model with diffusion*, J. Appl. Math. Comput., 217, (2010), pp. 3461–3479.
- [31] N. Shao, M. Zhong, Y. Yan, H. Pan, J. Cheng and W. Chen, *Dynamic models for Coronavirus Disease 2019 and data analysis*, Math. Methods Appl. Sci., 43, (2020), pp. 4943–4949.
- [32] G.Q. Sun, Z. Jin, Q.X. Liu and L. Li, *Spatial pattern in an epidemic system with cross-diffusion of the susceptible*, J. Biol. Systems, 17, (2009), pp. 141–152.
- [33] G.Q. Sun, S.F. Wang, M.T. Li, L. Li, J. Zhang, W. Zhang, Z. Jin and G.L. Feng, *Transmission dynamics of COVID-19 in Wuhan, China: effects of lockdown and medical resources*, Nonlinear Dynam., (2020), pp. 1–23.
- [34] P.F. Verhulst, *Notice sur la loi que la population suit dans son accroissement*, Corr. Math. Phys., 10, (1838), pp. 113.
- [35] B.G. Wang, W.T. Li and Z.C. Wang, *A reaction-diffusion sis epidemic model in an almost periodic environment*, Z. Angew. Math. Phys., 66, (2015), pp. 3085–3108.
- [36] J.O. Wertheim, A.J. Leigh Brown, N.L. Hepler, S.R. Mehta, D.D. Richman, D.M. Smith and S.L. Kosakovsky Pond, *The global transmission network of HIV-1*, J. Infect. Dis., 209(2), (2014), pp. 304–313.
- [37] M. Zagour, *Multiscale derivation of a time-dependent SEIRD reaction-diffusion system for COVID-19*, To appear in Modeling and Simulation in Science, Engineering and Technology, 2021.